Proving the antimicrobial therapeutic activity on a new copper-thiosemicarbazone complex

David Fabra, Georgiana Amariei, Daniel Ruiz-Camino, Ana I. Matesanz, Roberto Rosal, Adoracion G. Quiroga, Patricia Horcajada, Tania Hidalgo. Proving the antimicrobial therapeutic activity on a new copper-thiosemicarbazone complex. Molecular Pharmaceutics 21, 4, 1987-19977, 2024

https://doi.org/10.1021/acs.molpharmaceut.3c01235

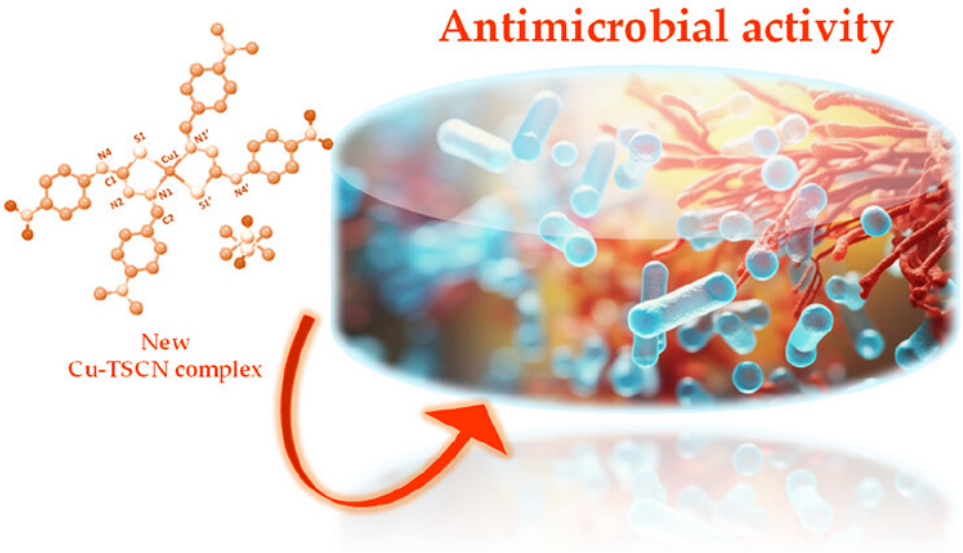

Proving the antimicrobial therapeutic activity on a new copper-thiosemicarbazone complex

David Fabra[1], Georgiana Amariei[2], Daniel Ruiz-Camino[1], Ángeles Aguilera[1], Ana I. Matesanz[1], Roberto Rosal[2] Adoracion G. Quiroga[1,*], Patricia Horcajada[3,*], and Tania Hidalgo[3,*]

[1]Department of Inorganic Chemistry, Universidad Autonoma de Madrid, Cantoblanco, 28049 Madrid, Spain
[2]Department of Chemical Engineering, University of Alcalá, 28871 Alcalá de Henares, Spain
[3]Advanced Porous Materials Unit (APMU), IMDEA Energy Institute, Ramón de la Sagra 3, 28935 Móstoles-Madrid, Spain

Abstract

The misuse and overdose of antimicrobial medicines are fostering the emergence of novel drug-resistant pathogens, providing negative repercussions not only on the global healthcare system due to the rise of long-term or chronic patients and inefficient therapies but also on the world trade, productivity, and, in short, to the global economic growth. In view of these scenarios, novel action plans to constrain this antibacterial resistance are needed. Thus, given the proven antiproliferative tumoral and microbial features of thiosemicarbazone (TSCN) ligands, we have here synthesized a novel effective antibacterial copper-thiosemicarbazone complex, demonstrating both its solubility profile and complex stability under physiological conditions, along with their safety and antibacterial activity in contact with human cellular nature and two most predominant bacterial strains, respectively. A significant growth inhibition (17 % after 20 h) is evidenced over time, paving the way toward an effective antibacterial therapy based on these copper-TSCN complexes.

1. Introduction

One of the top 10 global public health threats facing humanity is antimicrobial resistance (AMR) since the misuse and overdose of antimicrobial medicines are currently driving the appearance of novel drug-resistant pathogens, which could compromise crucial areas, such as global health, food safety and security, economic growth, poverty alleviation or, even, the environment [1]. This fact, in turn, not only leads to a raised emergence of untreatable common diseases (e.g., urinary infections, sepsis, diarrhea) but also poses larger life-saving medical procedures (e.g., ventilation, tube feeding, dialysis) riskier to be performed. This infection resistance has also been aggravated by the absence of new antibiotics on the pipeline market, resulting in long-term or chronic patients and inefficient therapies along with a high mortality index: in 2020, >800,000 people at all ages were infected in Europe (with 30 % of pediatric patients; 200,000 newborns), killing on average of 35,000 people per r [2].yea Thus, this circumstance led to a significant economic burden not only on the European healthcare system (estimated at ∼1.1 billion euro per year) but also on the global economy, international trade, healthcare, and productivity. Recently, the World Bank has estimated that if AMR is not addressed, the global economy may have lost ∼4 % of annual gross domestic product (GDP) by 2050, facing an estimated total cost of USD 100 trillion [3]. Given this ongoing situation and its future forecasting, European Commission has included a new Sustainable Development Goal (SDG) indicator, proposing recommended actions for fighting the AMR by 2030, as, for instance, (i) the creation of national plans for monitoring the antimicrobial consumption (AMC), (ii) the improvement of the infection prevention, (iii) the promotion of novel research and innovation plans or, even, (iv) the inspiration of the awareness raising among health professionals and/or the general public.

Thus, there is still plenty of room for improvement against this emerged pathological scenario. Some thiosemicarbazone (TSCN) copper (Cu)-containing complexes have been already tested for this purpose, focusing on a broad range of respiratory tract pathogens by delivering Cu ions efficiently into the cytoplasm of infected cells [4]. In fact, just the TSCN has been used for the treatment of diverse human diseases, including cancer [5,6] or tuberculosis [7]. Related compounds, such as p-acetamidobenzaldehyde thiosemicarbazone (amithionoze©) already at the second World War (in Africa and South America), showed bacteriostatic efficiency on Mycobacterium

* Corresponding authors: adoracion.gomez@uam.es, patricia.horcajada@imdea.org, tania.hidalgo@imdea.org
Available online: March 20, 2024

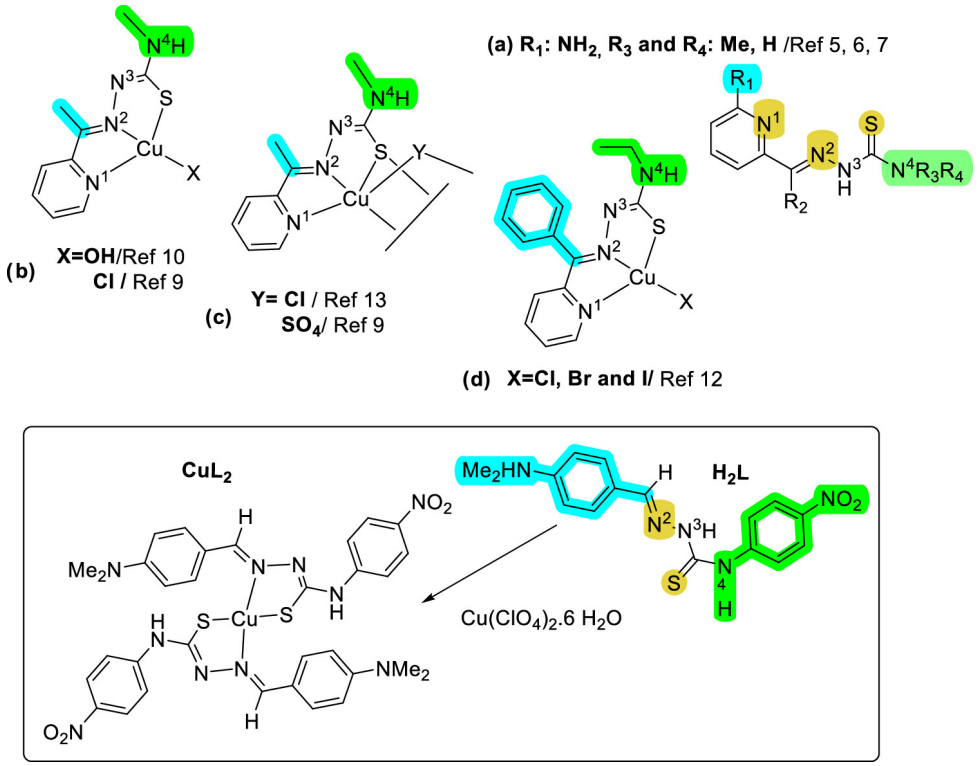

Figure 1: *Thiosemicarbazone and copper complexes with similar structures and antibacterial activity.*

tuberculosis in combination with isoniazid [8], and in general, those TSCN with better lipophilicity and available binding sites showed the best performance (Figure 1a, binging sites highlighted in yellow) [5]. Thereafter, this TSCN's effectiveness has been improved in some cases with copper metalation (mononuclear complexes; Figure 1b; X:Cl and dinuclear compounds; Figure 1c; Y = SO_4) [9], achieving even synthetic fibers with excellent growth inhibition by grafting antibacterial copper TSCNs onto cellulose (Figure 1b; X:OH) [10].

The experimental data about the TSCN complexes' mechanism and stability in physiological solution are quite scarce, despite their efficacy has been generally reported mostly for mononuclear tridentate complexes (Figure 1c; X:OH, Cl, and even bipy [11]) and/or some dinuclear (Figure 1b, Y: μ-SO_4, (9) μ-Cl, [12]), which has been ascribed to the lessening of metal toxicity: turning to a more lipophilic character (i.e., bisthiosemicarbazones) [4], and ligand release. This action leads to an antibacterial effect [13]: increase of reactive oxygen species (ROS) generation [14], associated with potential DNA damage [15] and also binding with target antibacterial proteins (Figure 1d; R is aromatic [12] but also contains aliphatic groups [16]). From the recent literature, the substitution at the terminal N4 group of TSCN seems to boost the complex lipophilicity, enabling a greater diffusion through the lipid bacterial wall and, in turn, enhancing the antibacterial activity with lower side effects [12]. No other structure-activity relationship or other obvious additional role of copper complexes have been clearly established from the reported data up to now. This is a clear indication of the need of a more detailed comparison from the variety of examples with these molecules, their complexes, and the methodologies used in the antibacterial analysis [17].

In view of the above, the actual social needs, and our previous experience producing effective anticancer complexes using TSCN by a groove-binding model [18], we propose here an innovative antimicrobial copper therapeutic agent based on a similar TSCN with N4 substitution, H_2L (N1-(4-(dimethylamino)benzylidene)-N4-(4-nitrofenil)thiosemicarbazone, Figure 1). In this respect, the antibacterial efficacy of this $Cu(HL)_2$complex is evaluated using two diverse strains, widely recognized as appellant human pathogenic models with broadly propagation features: (i) *Escherichia coli* (*E. coli*; EC), the main representative of Gram-negative bacterial strains resistant to third-generation cephalosporins, and (ii) *Staphylococcus aureus* (*S. aureus*; SA), a Gram-positive strain, part of our own skin flora and with a frequent occurrence in healthcare facilities. Among others, it creates resistance against the medicine methicillin, a derivative of the popular penicillin (e.g., sensitive infected patients are more likely to decease in 64 % times higher than nonresistant ones) [19]. In addition, we report our findings from the studies of the solu-

tion profile of this Cu-TSCN complex in biological media, its integrity, and in vitro biosafety character, which is crucial for reliable and reproducibility data.

2. Experimental section

2.1. Methods

NMR spectra were recorded at room temperature, using a two-channel 300 MHz Bruker Avance III-HD Nanobay spectrometer equipped with a 5 mm BBO 1H/X probe and Z gradients, located at the Interdepartmental Investigation Service (SIdI). DMSO-d6 was used as the solvent (containing 0.05 % (v/v) tetramethylsilane (TMS) as a reference). Chemical shift values are given in parts per million (ppm) relative to the residual TMS signals. The following abbreviations were used: s (singlet), d (doublet), and m (multiplet). Elemental analyses were performed on a LECO CHNS-932 elemental analyzer located at SIdI. Mass spectra were recorded using fast atom bombardment (FAB) in a Waters VG AutoSpec mass spectrometry unit and using matrix-assisted laser desorption/ionization (MALDI) with a Bruker Ultraflex III (MALDI-TOF/TOF) mass spectrometry unit, both located at SIdI. Infrared (IR) spectra were recorded using a PerkinElmer Model 283 spectrometer with an attenuated total reflectance (ATR) MIRacle Single Reflection Horizontal accessory and equipped with CsI optical windows for spectra between 600 and 200 cm^{-1} in Nujol mull preparations. Absorbance spectra and UV-visible spectra were recorded using a Thermo Evolution 220 spectrophotometer equipped with temperature control within ± 0.1 °C.

For particle size and ζ-potential determinations, each complex was diluted from the dimethyl sulfoxide (DMSO) stock (5 mM) with the desired media (aqueous solution, cell culture media; see Section 3, nutrient broth-NB medium, composed by 5 g L^{-1} beef extract, 10 g L^{-1} peptone, 5 g L^{-1} NaCl, pH = 7-7.2), being analyzed with a Malvern Nano-ZS, Zetasizer Nano series. Once the suspensions were prepared, an ultrasonication step followed (ultrasound tip at 10 % amplitude for 1 min), monitoring the particle size evolution from t = 0 to 24 h. The studies were performed with 1 % DMSO (v/v) in the final solution.

2.2. H_2L Synthesis

2.2.1. *Precursor*

p-Nitrophenylthiosemicarbazide was prepared following a reported procedure [20] with slight changes in the purification procedure. Briefly, on a suspension of p-nitrophenylsothiocyanate (1.0043 g, 5.57 mmol) in acetonitrile (20 mL) cooled in an ice bath, a solution of hydrazine hydrate (541.8 μL, 11.1 mmol) in acetonitrile (15 mL) was added dropwise, and the reaction was kept with constant stirring for 1 h, obtaining a brown solid that was filtered, washed with acetonitrile, and vacuum-dried. The product was purified by chromatography on silica gel, using CH_2Cl_2 and CH_2Cl_2/EtOH (99:1) as eluents. The final product was eluted last and concentrated to dryness, isolating 712.6 mg of a yellow solid. Yield: 60 %. FAB$^{\pm}$-MS (*m/z*): $[M + CH_3CN]^+$: 253. ^{1}H-RMN (300 MHz, DMSO-d_6), δ(ppm): 8.07 (d, 2H, H_6); 8.21 (d, 2H, H_7); 10.26 (s, 1H, N-H_2); 10.76 (s, 1H, N-H_4). ^{13}C-RMN (DMSO-d_6), δ(ppm): 123.45 (C_7), 123.70 (C_6), 143.06 (C_8), 145.45 (C_5), 175.74 (C_3). IR (cm^{-1}): ν_a (NH_2): 3336; ν_s (NH_2): 3241; ν (NH): 3211; δ (NH_2): 1637; ν_a (NO_2): 1506; ν_2 (NO_2): 1334; ν (C=S): 848 (Figure S1, NMR numbering).

2.2.2. *H_2L:N1-(4-(dimethylamino)benzylidene)-N4-(4-nitrofenil)thiosemicarbazone*

H_2L was prepared following a reported procedure [20] with important variations that are described as follows: an ethanolic solution (1.5 mL) of p-dimethylaminobenzaldehyde (11.3 mg, 0.076 mmol) was added dropwise to a solution of p-nitrophenylthiosemicarbazide (16.1 mg, 0.076 mmol) in AcOH 6 % (2 mL) at 50 °C. The mixture was stirred and heated to reflux temperature for 5 h. An orange solid was isolated after cooling by filtration and washed several times with very cold portions (5 mL) of ethanol and cold methanol. Finally, the solid (17.2 mg) was recrystallized into CH_2Cl_2, filtered, and vacuum-dried. Yield: 66 %. Orange solid. Elemental analysis (%) for $C_{16}H_{17}N_5O_2S{\cdot}H_2O$: Calculated: C, 53.17; H, 5.30; N, 19.38. Experimental: C, 52.51; H, 4.81; N, 19.27. FAB$^{\pm}$-MS (*m/z*): $[M]^+$: 343.2; $[M+H]^+$: 344.2. ^{1}H-RMN (300 MHz, DMSO-d_6), δ(ppm): 2.98 (s, 6H, H11); 6.74 (d, 2H, H9); 7.70 (d, 2H, H8); 8.10 (d, 3H, H2 and H6); 8.23 (d, 2H, H3); 10.29 (s, 1H, N-HA); 11.96 (s, 1H, N-HB). ^{13}C-RMN (DMSO-d_6), δ(ppm): 39.52 (C11), 111.59 (C9), 120.70 (C7), 123.59 (C2), 123.64 (C3), 129.31 (C8), 143.13 (C1), 145.25 (C6), 145.62 (C4), 151.75 (C10), 174.03 (C5). IR (cm^{-1}): ν (NH): 3254, 3118; ν (C=N): 1611; ν_a (NO_2): 1501; ν_s (NO_2): 1330; ν (C=S): 843 (Figure S1, NMR numbering).

2.3. Synthesis of the Cu complex

H_2L (50.06 mg, 0.146 mmol) was suspended in methanol (50 mL), and a NaOH (0.1M) solution was added until the mixture turned into a clear solution at pH 9. Then, a solution of $Cu(ClO_4)_2{\cdot}6H_2O$ (39.41

mg, 0.106 mmol) in 5 mL of methanol was added dropwise at room temperature. The reaction mixture was stirred for 24 h, turning olive green to dark brown. The solid obtained was filtered, washed with water and MeOH, and vacuum-dried (40.89 mg). The recrystallization of the compound in DMSO afforded monocrystals suitable for X-ray diffraction [$Cu(HL)_2$]. Brown solid. Yield: 75 %. Single crystals were obtained from a DMSO solution of the pure complex. Elemental analysis (%) for $C_{32}H_{32}N_{10}O_4S_2Cu{\cdot}4H_2O$: Calculated: C, 46.85; H, 4.91; N, 17.07. Experimental: C, 47.06; H, 4.27; N, 16.98. IR (cm^{-1}): ν (NH): 3392; ν (C=N): 1606; ν_a (NO_2): 1482; ν_s (NO_2): 1323; ν (C-S): 807. Lattice water molecules exhibit bands at 3550-3200 cm^{-1}; δ: 1630-1600 cm^{-1}; and librational modes: 600-200 cm^{-1}. Thermogravimetric analysis (TGA) indicates the release of one water molecule at 175 °C and decomposition between 175-400 °C.

2.4. Crystallography data

Data were collected on a Bruker Kappa Apex II diffractometer. A summary of the crystal data, experimental details, and refinement results is listed in Table 1. The software package SHELXTL was used for space group determination, structure solution, and refinement [21]. The structure was solved by direct methods, completed with difference Fourier synthesis, and refined with anisotropic displacement parameters.

2.5. Lipophilicity measurements

The lipophilicity of the compounds was determined by measuring their log *P* in a n-octanol/Tris-buffered aqueous solution with a pH of 7.40. The ligand H_2L and the corresponding Cu complex were dissolved in n-octanol (previously saturated with aqueous buffer), and the same volume of aqueous buffer (presaturated with octanol) was added to n-octanol. The samples were thoroughly mixed with stirring for 1 h and, then, the two phases were separated by means of centrifugation at 6000 rpm for 5 min. Following the phase separation, UV-Vvis spectra of the compounds were recorded in both the n-octanol and aqueous phases. These spectra were then compared to those of the original n-octanol stock solutions. Experiments were carried out in triplicate, and the log *P* values of the compounds were determined using the following Eq. 1.

$$logP = log\frac{[compound]_{oct}}{[compound]_{water}} = log\left(\frac{A_{oct}}{A_{aq.}}\right) \quad (1)$$

2.6. Structural stability

2.6.1. UV-Visible monitoring in buffer solution

The compound was initially dissolved in DMSO (5 mM). For all experiments, the desired concentration of complexes was achieved by dilution of the stock DMSO solution with Tris-HCl aqueous buffer to reach the concentration of complex from 10^{-6} to 10^{-4} M. All of the solutions and buffers were adjusted to pH 7.40 and 37 °C. The studies were performed with 1 % DMSO (v/v) in the final solution.

2.6.2. UV/Vis Kinetics Experiments with Hen Egg White Lysozyme (HEWL)

To investigate the interaction of complex Cu(HL)2 with model proteins, electronic spectra of the protein model HEWL at 3.33×10^{-6} M dissolved in Tris-HCl (pH 7) were recorded. The typical absorbance of proteins at 280 nm was monitored before and after the addition of complex $Cu(HL)_2$ using 2.5 % DMSO at a stoichiometric ratio of 3:1 (metal to protein) for 24 h at room temperature. The binding affinity constants were calculated as a pseudo first order based on the equal results obtained for stoichiometry of 10:1 and 3:1 for both cases.

2.7. Cyclic voltammetry

Cyclic voltammetry assays were carried out in a three-electrode cell: 1- and 2-platinum as the working and counter electrodes and 3-Ag/AgCl containing KCl (3M) as the reference electrode. Measurements were performed at room temperature using a biopotentiosat (μStat 400 bipotentiostat/galvanostat STAT 400). Deaeration of the solutions was accomplished by passing a stream of nitrogen through the solution for 10 min prior to the measurement, maintaining a blanket N_2 atmosphere over the solution during the measurement. The potentials were measured using a 10^{-3} M solution of complex in a mixture of solvents of dimethylformamide (DMF)/PBS (2:1 v/v) at pH 7.4 containing 0.10 M [n-Bu_4N][BF_4] as the supporting electrolyte.

2.8. Safety: cell culture and cellular viability (MTT assay)

Human colon (Caco-2, ATCC HTB-37) carcinoma cell line and the promyelocytic cell line HL-60 (ATCC CCL-240) were maintained in DMEM (the first cell line) and RPMI medium (last one), respectively, supplemented with glutamax-1 with 10 % of heat-inactivated FBS, 1°,% penicillin/streptomycin, 1 %

Table 1. *Crystal Data, Experimental Details, and Refinement Results for the Crystal Resolution of Cu(HL)$_2$ [a].*

Chemical formula	$C_{36}H_{44}CuN_{10}O_6S_4$		
Formula weight (g mol^{-1})	904.59		
Temperature (K)	200(2)		
Crystal system	triclinic		
Wavelength (Å)	0.71073		
Space group	$P\bar{1}$		
Crystal size (mm^3)	0.046 × 0.056 × 0.156		
a (Å)	α (deg)	12.6904(5)	103.4707(18)
b (Å)	β (deg)	13.1423(4)	110.8505(18)
c (Å)	γ (deg)	13.8468(5)	93.2278(18)
Volume (Å^3)	Z 2074.00(13) 2		
Density, calculated (g cm^{-3})	1.449		
Absorption coefficient (mm^{-1})	0.785		
F(000)	942		
θ range for data collection (deg)	1.61-25.35		
Reflections collected	94931		
Independent reflections	7569 [$R_{(int)}$ = 0.1246]		
Coverage of independent collections	99.6 %		
Data/restrains/parameters	7569/6/530		
goodness of fit on F^2	1.064		
Final R indices [I > 20(l)]/all data	R_1 = 0.0488/0.1015		
	wR_2 = 0.1114/0.1357		
Largest diff. peak and hole (e/Å^{-3})	0.448 and -0.406		

[a] All details can be found in CCDC 2119427, which contain the supplementary crystallographic data for this paper. These data can be obtained free of charge from The Cambridge Crystallographic Data Center via `https://summary.ccdc.cam.ac.uk/structure-summary-form`

l-glutamine, and 1 % nonessential amino acids. Both cell lines were routinely grown at 37 °C in a humidified 5 % CO_2 atmosphere. Media were changed twice per week and cells were passaged at 80 % of confluence (cell density at 8 × 10^4, ∼1 × 10^5 cells per cm^2), being harvested by trypsinization (1 % trypsin-EDTA solution).

The cytotoxic activity of the [Cu(HL)$_2$] complex as well as its precursors (91.55 % of H_2L and 8.5 % of $CuCl_2{\cdot}2H_2O$, respectively) were analyzed by the colorimetric 3-(4,5-dimethylthiazol-2-yl)-2,5-diphenyltetrazolium bromide (MTT) assay. The adherent colon cell line (Caco-2 cells) and the suspension HL-60 cells were seeded 24 h prior to the assay in 96-well plates at a density of 1 × 10^5 cells per well in supplemented culture media. The complex suspensions were prepared as a dilution series with cell culture media described as follows: 30 μL of each complex [from a stock prepared at 1 % DMSO aqueous solution (v/v)], was added to a final volume of 300 μL per well, yielding different concentrations ranging from 10 to 0.08 μM (in triplicate). Moreover, a set of diverse control wells was left on each plate: (i) medium without cells, (ii) cells with a cytotoxic agent (Triton), (iii) untreated cells, and (iv) cells containing medium with the same concentration of DMSO (DMSO control). Subsequently, all of these treatments were added into the cells for 72 h while being kept at 37 °C with a 5 % CO_2 atmosphere. The cytotoxicity was determined by adding the MTT reactant (0.5 mg mL^{-1} in PBS, incubated at 37 °C for 2 h) followed by PBS washing with 100 μL, ending with 100 μL of DMSO added to each well. Absorbance was determined at λ = 539 nm under stirring. The percentage of cell viability was calculated by the absorbance measurements of control growth and test growth in the presence of the formulations at various concentration levels.

2.9. Antibacterial activity

Two standard bacterial strains were used as representative of Gram-positive type, *S. aureus*-SA (CECT 240, strain designation ATCC 6538P), and Gram-negative, *E. coli*-EC (CECT 516, strain designation ATCC 8739) for the antibacterial performance, preserved at -80 °C in glycerol (20 % v/v) until their use. For their reactivation, 1 mL of each inoculum was resuspended in nutrient broth under stirring conditions (NB, 20 mL, 37 °C, 100 rpm), being routinely tracked by measuring the optical density (OD) at 600 nm (Shimadzu UV-1800 spectrophotometer) in order to preserve the

exponential phase of each microorganism during the total contact time (20 h). In particular, diverse concentrations of $[Cu(HL)_2]$ solutions (0, 13, 17, 33, 67, 100, and 134 μM) were prepared as well as control samples (H_2L ligand and $CuCl_2{\cdot}2H_2O$), being dissolved over 2.4 mL of the previously mentioned 106 cells mL^{-1} inoculums of a 24-well plate. In the case of the controls, for each desired concentration, the quantity of each constituent was adjusted to the corresponding part of the bulk unit (e.g., 17 μM $[Cu(HL)_2]$ corresponds to 15.4 μM H2L + 4.0 μM $CuCl_2{\cdot}2H_2O$). After 20 h of incubation at 37 °C under static conditions, the bacterial viability was evaluated by determining the following parameters:

(A) Colony-forming units (CFU), where 10-fold serial bacteria dilutions in PBS were placed in sterile 96-well plates. Replicated 10 μL spots were placed on Petri dishes containing NB agar medium, and the CFU was counted after 24 h using a CL-1110 counting instrument (Acequilabs, Spain). For colony number estimations, at least three replicates of at least two serial dilutions were considered in order to obtain an estimated inhibition (CFU mL^{-1}).

(B) Fluorescein diacetate staining (FDA) is a nonfluorescent compound, extensively used as an indicator for *S. aureus/E. coli* enzymatic activity determination due to its ability to turn to a green fluorescent agent (fluorescein) once metabolized by functional cells. Thus, this enzymatic conversion was analyzed in 96-well black microplates by mixing 5 μL of FDA (2 mg mL^{-1} in DMSO) with 195 μL of bacterial suspension in each well. The plate was incubated at 25 °C for 30 min with continuous readings every 5 min (λ_{ex} = 485 nm; λ_{em} = 538 nm) using a fluorometer (Fluoroskan Ascent FL Fluorimeter/Luminometer; Thermo Scientific, Waltham, MA). The possible fluorescence interference of the culture medium and $[Cu(HL)_2]$ was also checked [22]. Each sample was measured for quadruple, disclosing the outcomes as an inhibition percentage and normalizing the difference of the sample fluorescence intensity with the control blank assays.

Moreover, the fluorometer was also used for the determination of bacterial oxidation (ROS production) [23,24]. Briefly, 150 μL of each sample fraction was incubated for 30 min in 96-well black microplates with 50 μL of 10 mol L^{-1} of the ROS salt (2′,7′-dichlorodihydrofluorescein diacetate, H_2DCF-DA), which is sensitive for hydrogen peroxide and other oxidative species, including hydroxyl and peroxyl radicals. Each sample was measured for quadruple readings every 5 min (λ_{ex} = 495 nm; λ_{em} = 525 nm) and represented normalized with respect to the negative control group for a direct comparison.

Confocal laser scanning microscopy (CLSM) was performed for visual and qualitative assessment of antibacterial performances. Cell images of each bacteria strain were obtained after contact with the $[Cu(HL)_2]$ suspensions (50 μL aliquot) via confocal microscopy using a Confocal SP5 (Leica Microsystems, Germany). The bacteria were stained with a LIVE/DEAD kit (Live/Dead BacLight Viability Kit, Thermo Fisher), where 10 μL of the fluorescent dye mixture [10 μL of propodium iodide (PI) + 10 μL of Syto 9 in 980 μL of DMSO] was incubated with each bacterial strain during 30 min at RT (in the dark). Green fluorescence determines the "live" bacteria (intact membrane; Syto 9: live cells, λ_{ex} = 480 nm; λ_{em} = 500 nm), whereas the red intensity indicates the "dead" cells (PI: dead cells, λ_{ex} = 490 nm; λ_{em} = 635 nm).

2.10. Statistics

The results of different assays are represented as the mean ± standard deviation (SD). Ordinary two-way analysis of variance (ANOVA) followed by Tukey's multiple comparison tests was carried out to determine significant differences using GraphPad Prism 9.2 software (GraphPad Software, Inc., La Jolla, CA). Each experiment was performed at least three times ($n \geq 3$). In the graphs, the results are indicated as $^{*}P \leq 0.05$, $^{**}P \leq 0.01$, $^{***}P \leq 0.001$, and $^{****}P \leq 0.0001$.

3. Results and discussion

3.1. Synthesis and characterization of Cu(II) complex

The Cu(II) complex was synthesized by the reaction between $Cu(ClO_4)2{\cdot}6H_2O$ and H_2L in a stoichiometric ratio of 1:2. The elemental analysis data of complex 1 are in accordance with the general formulas: $Cu(HL)_2$. In the IR spectrum of the complex, significant changes are found in comparison with the free ligand; one of the ν(NH) bands disappears, indicating ligand deprotonation, and the ν(C=N) band is found at lower frequencies, which supports that the coordination of Cu(II) has taken place through the nitrogen of the iminic group. The ν(C=S) band also disappears, and a new band arises at the region of ν(C-S) bands, which supports that the TSCN coordinates to the metal in its thiolate form. Indeed, the presence of water molecules in the complex structure is supported by Fourier transform infrared spectroscopy (FTIR) spectrum (e.g., antisymmetric and symmetric OH stretching at 3550-3200 cm^{-1}; HOH bending at 1630-1600 cm^{-1}; also, "librational modes" as consequences of rotational oscillations, restricted by the neighboring atomic interactions at 600-200 cm^{-1}) since some

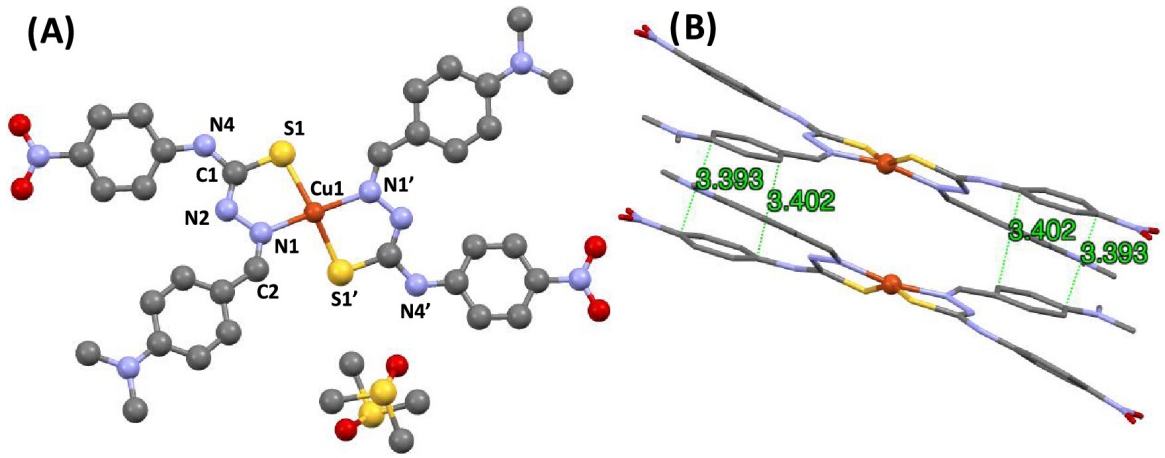

Figure 2: *(A) Molecular structure of complex Cu(HL)$_2$ showing the atom numbering of the TSCN core. Hydrogen atoms have been omitted for the sake of clarity. (B) Molecular arrangement in the complex crystal structure.*

of the water molecules are not detectable by TGA (Figure S2) [25]. The proposed structure, based on analytical and spectroscopic data [25], was confirmed by single-crystal X-ray diffraction (Figure 2). The geometry around the central ion is a distorted square plane, with two deprotonated TSCNs bound in trans configuration forming two five-membered chelate rings through the S and N donor atoms.

The Cu-N and Cu-S binding distances (Table 2) are comparable with those of other reported Cu(II)-TSCN complexes. The C-S bond distance at the coordinated ligand ($\sim$ 1.74 Å is within the expected range for a single bond, confirming the thiolate TSCN's form [27,28]. The C-N and N-N distances are intermediate between single and double bonds, confirming that charge is delocalized along the TSCN skeleton (Figure 2A) [29,30].

Table 1: ***Table 2.*** *Selected Bond Distances and Angles for Complex Cu(HL)$_2$[a].*

bond distances (Å)		bond angles (deg)	
Cu1–S1	2.2337(11)	N1–Cu1–S1	85.02(9)
Cu1–N1	1.990(3)	N1–Pd1–S1′	96.11(9)
C1–S1	1.742(4)	N1–Pd1–N1′	168.61(12)
C1–N2	1.298(4)	S1–Pd1–S1′	159.14(6)
C2–N1	1.294(5)		
N1–N2	1.394(3)		

[a] Numbering included in Figure 2.

The crystalline packing of complex 1 is stabilized by intermolecular hydrogen bonds between solvent molecules (dimethyl sulfoxide, DMSO) and N4 of the ligands (N4$\cdots$O = 2.794(4) Å) and, in addition, by the existence of a certain π-π stacking between the aromatic rings of adjacent molecules with 3.393 Å (Figure 2B).

3.2. Complex stability in buffered solutions

Speciation of metallic drugs in solution is known to increase in complexity with the use of coordinating solvents, such as DMSO, or more complex buffers, such as simulated physiological media (Tris-HCl, phosphate-buffered solution (PBS), culture media, etc.), where the presence of diverse biological components (e.g., proteins, salts, electrolytes) could impact the complex solubility and/or charge, which could compromise their performances. In some cases, the solvent can cause inactivation [31–34] or the production of new species, which may affect its efficiency [18,35]. Hence, the identification of active species or the investigation of the physicochemical features under relevant environments (mainly structural and colloidal stability) has become a mandatory study for the evaluation of potential therapeutically active drugs. In order to shed light on its biological activity and suitability for the desired antimicrobial purposes, the stability profile of the Cu(HL)$_2$ complex was monitored in diverse physiological media up to 24 h, starting from the simplest, such as aqueous solution (containing 1% of DMSO) or Tris-HCl/DMSO, to more complex ones, such as culture media (cellular or bacterial nutrient broth, NB), by using UV-visible spectroscopy for the structural stability (see Section 3.1 and 3.2) or dynamic light scattering (DLS) for the colloidal stability (Section 1 and Table S1). A broad range of concentrations (up to 45 M, Figure 3A) were tested, showing a very slight decrease in absorbance at 6 h, which was maintained up to 24 h. This behavior is also in agreement with the observed hydrodynamic particle size and ζ-potential values determined by DLS: here, the complex displayed a monodispersed size of 69 $\pm$ 22 with a negatively charged surface of -22 $\pm$ 2 mV, maintaining its col-

loidal performance after longer incubations times in aqueous solution (76 ± 26 nm and -22 mV at 24 h, respectively; Table S1).

Once we have learned about the solution behavior of the compound, we study the lipophilicity of the ligand H_2L and the Cu complex $Cu(HL)_2$ for a better understanding of their potential permeability and metabolism impact (e.g., absorption, distribution, metabolism, and excretion (ADME)), which, in turn, affect their potency, selectivity, and/or toxicity [36]. This key parameter is determined by their log *P* values using Tris buffer as a model for the aqueous phase, a common medium to sustain the bacterial growth (i.e., pH control) [37]. In both cases, the compounds showed a greater lipophilicity than 1 (log *P* values of 2.08 ± 0.03 and 2.95 ± 0.07 for H_2L and $Cu(HL)_2$, respectively), being slightly higher for the complex, which might be considered as positive for its potential cell internalization [4]. Generally, a compound with an average log *P* level between 1 and 4 is considered more likely to possess optimal ADME physicochemical features for their therapeutic performances [38].

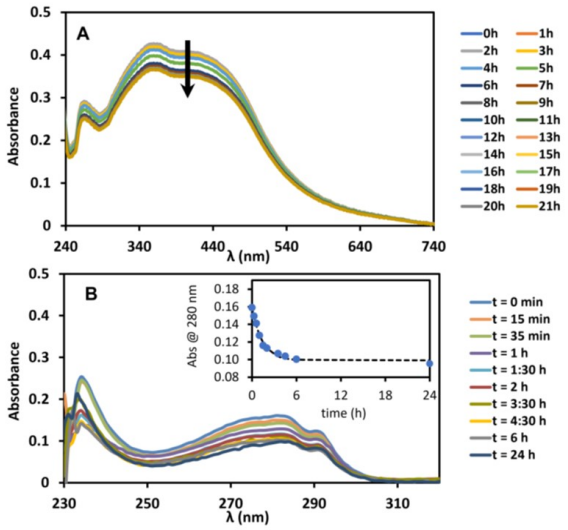

Figure 3: *(A) UV–visible spectra of Cu(HL)2 monitored from fresh to 24 h. (B) UV/vis absorption data of the complex $Cu(HL)_2$ with lysozyme over time and its binding rates (ratio used 3:1), plotted with the absorbance progress at λ = 280 nm monitored from fresh to 24 h.*

For the microbial assays, we have investigated more complex scenarios. Usually, any material (including metallodrugs) dispersed in culture media strongly interact with proteins as a second biological target, adsorbing them on their surface (forming the so-called protein corona), which affects their surface charge and, consequently, their stability and/or biodistribution [39,40]. As depicted in Table S1, this copper complex in the presence of the NB bacterial components (e.g., beef extract, peptone) exhibited an increase of the particle size, displaying a higher aggregation after 24 h (142 vs 241 nm, respectively). On the other hand, when they interact with cell culture media (e.g., serum, antibiotics), $Cu(HL)_2$ seemed to partially stabilize the size maintaining the nanometric range in a fresh solution, which slightly reach some aggregation after longer contact times (52 vs 125 nm). In both cases, the protein corona formation was also confirmed by the ζ-potential shift from a negative charge in aqueous solution to more neutral values at both incubation times. A more neutral surface could explain the aggregation, observing similar colloidal performances in recently reported TSCN-based Pd complexes [18].

In terms of structural stability of metal complexes acting as potential drugs, a broadly applicable protein model for evaluating metallodrug–protein interactions (the hen egg white lysozyme (HEWL) by UV–Vis, electrospray ionization (ESI) mass spectrometry, or X-ray) [41–43] is available. Highly positively charged with hydrophobic residues, HEWL is known as a suitable protein model for biological active binding examination, [44] giving insights into potential aggregation processes in body fluids. Thus, we assess any potential change produced in the UV spectrum of this lysozyme after the interaction with the $Cu(HL)_2$ complex upon its dispersion in aquo-buffered solution. In this case, the kinetic constant was determined as a pseudo-first-order reaction plotting the absorbance values at 280 nm (the characteristic absorption of proteins) as a function of time and fitted to an exponential function (Figure 3B). The resulting absorbance of $Cu(HL)_2$-HEWL showed a progressive intensity decrease up to 24 h, very similar to the observed rate of the cisplatin-HEWL control model (45) being also within the range of other similar complexes with the β-amyloid special interaction reported previously by some of us [18]. Thus, $Cu(HL)_2$ seems to possess adequate quality stable values in the desired physiological media.

3.3. Electrochemical profile

For unveiling the redox potential performance, the electrochemical behavior of the $Cu(HL)_2$ complex was investigated by cyclic voltammetry, undertaking the measurement in the most similar condition to the cellular environment, requiring a mixture of solvents [e.g., DMF/PBS, pH 7.4 (2:1 v/v; following reported procedures) due to its low aqueous solubility]. The complex exhibited an irreversible reduction peak at (-0.64 V) vs Ag/AgCl (Figure S4) that could be attributed to a CuII/I process. This value correlates to (-0.43 V) vs NHE (normal hydrogen electrode), which is more negative than the reported redox potentials of common biological reducing agents as,

for instance, AA (ascorbic acid; +0.06 V), NAC (N-acetylcysteine; -0.18 V), or GSH (reduced glutathione; -0.24 V). Another pseudoreversible process at more positive potentials ($E°_{1/2}$ 0.37 V in Ag/AgCl) has been displayed by the complex, which can be related to this CuIII/II process. Although it has been very difficult to establish a direct and/or accurate comparison with reported data (slight difference of the experimental setup) [46], the obtained redox potential suggests that the $Cu(HL)_2$ complex could display resistance to the in vivo reduction [47]. Moreover, some authors have found similar values with copper square planar thiosemicarbazone (NNSS donors) complexes, suggesting also its ineffectiveness role for this redox activity [48].

3.4. Antibacterial activity

The treatment of human infectious diseases is currently running out of effective antibiotics due to extensive misuse or overuse, which has promoted an increased rate of bacterial infection (mostly in the bloodstream), as, for instance, the case of the *E. coli*- or *S. aureus*-resistant strains to popular and prescribed medicines, such as cephalosporins or penicillin derivatives. Thus, the development of novel action plans to constrain this AMR spreading has been highlighted by the World Health Organization (WHO) [3]. In view of this emerging concern and taking into account the steady $Cu(HL)_2$ stability, the potential antimicrobial approach of this metallodrug has been explored, selecting *S. aureus* and *E. coli* as pathogenic bacterial models. However, prior to these assays, we studied the potential biosafe dose of this complex in the presence of 2 diverse cell lines, both healthy and cancerous nature: (1) the colon adenocarcinoma Caco-2 cells ("colorectal cancer"), as the third most frequent type of cancer and well-characterized intestinal barrier model, extensively used over the past few years for preclinical studies of diverse therapeutic agents, and (2) the immunological HL-60 cell line involved in relevant biological processes, such as the cellular redox homeostasis (ROS). After 72 h of contact, a potential concentration-dependent cytotoxic effect was evidenced, the most elevated doses of $Cu(HL)_2$ (from 1.25 to 10 μM; Figure S3) being mainly responsible to decrease the cellular viability, regardless of the cell origin. These findings are in agreement with previously reported antiproliferative TSCN ligand activity derived from Cu(II) complexes, obtained by others, showing higher Caco-2 cytotoxicity after 48 h (IC50 range of 0.68-1.07 μM) [13]. Thus, these outcomes underlined the need to select a specific complex concentration range in order to achieve an effective performance with minimal side effects.

Bearing this in mind, diverse doses of $Cu(HL)_2$ were tested for effective antimicrobial selection, evaluating both the colony-forming units (CFU) and the microbial enzymatic activity by the fluorescein diacetate hydrolysis assay (FDA) in contact with SA and EC bacteria (see Section 4 for further details). After distinct incubation times (3, 6, and 20 h) in contact with a serial dilution of the complex (from 0 to 134 μM), a remarkable effect was observed for both strains: a statistically significant growth inhibition of ~22 and 12 % in SA and EC after 20 h was reached, respectively (see Figure S5; $p < 0.001$). This high inhibition percentage (bordering CFU values of 0; $p < 0.05$) was provided by the MIC, namely, as the minimum inhibitory concentration needed to prevent the bacterial growth, which was estimated by 13 and 33 μM $Cu(HL)_2$ for SA and EC, respectively.

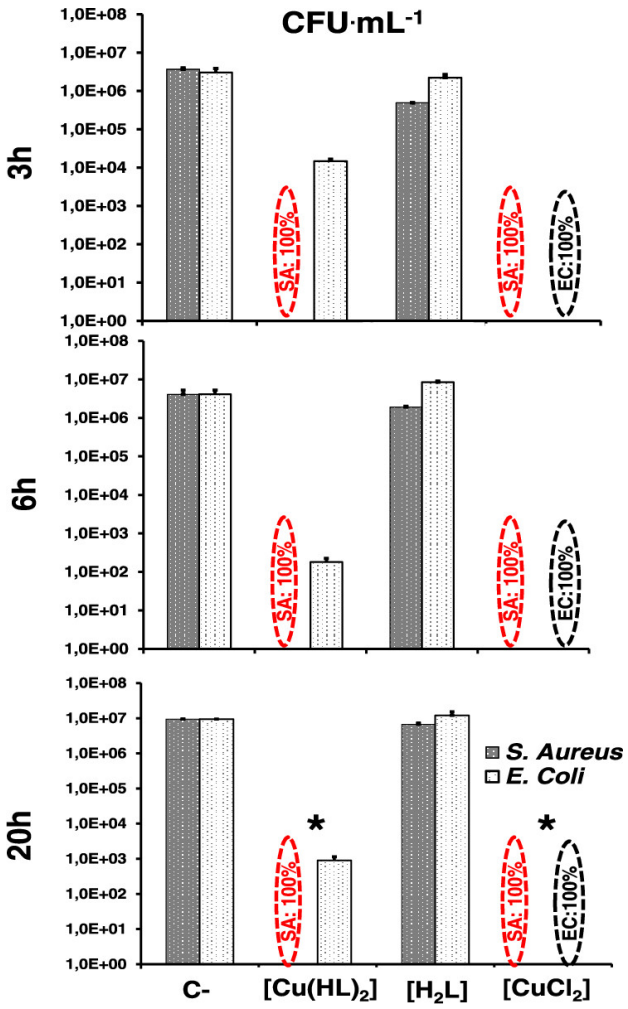

Figure 4: *Colony-forming unit of S. aureus (dark column) and E. coli (white column) after 3, 6, or 20 h of contact with the selected active [$Cu(HL)_2$; 17 μM] concentration together with the corresponding amount of the following controls: free H_2L ligand and $CuCl_2{\cdot}2H_2O$ precursor. In all cases, each sample value was normalized with a negative control (C-, 100 % of bacterial viability). The statistical significance was disclosed as* $^*p < 0.05$.

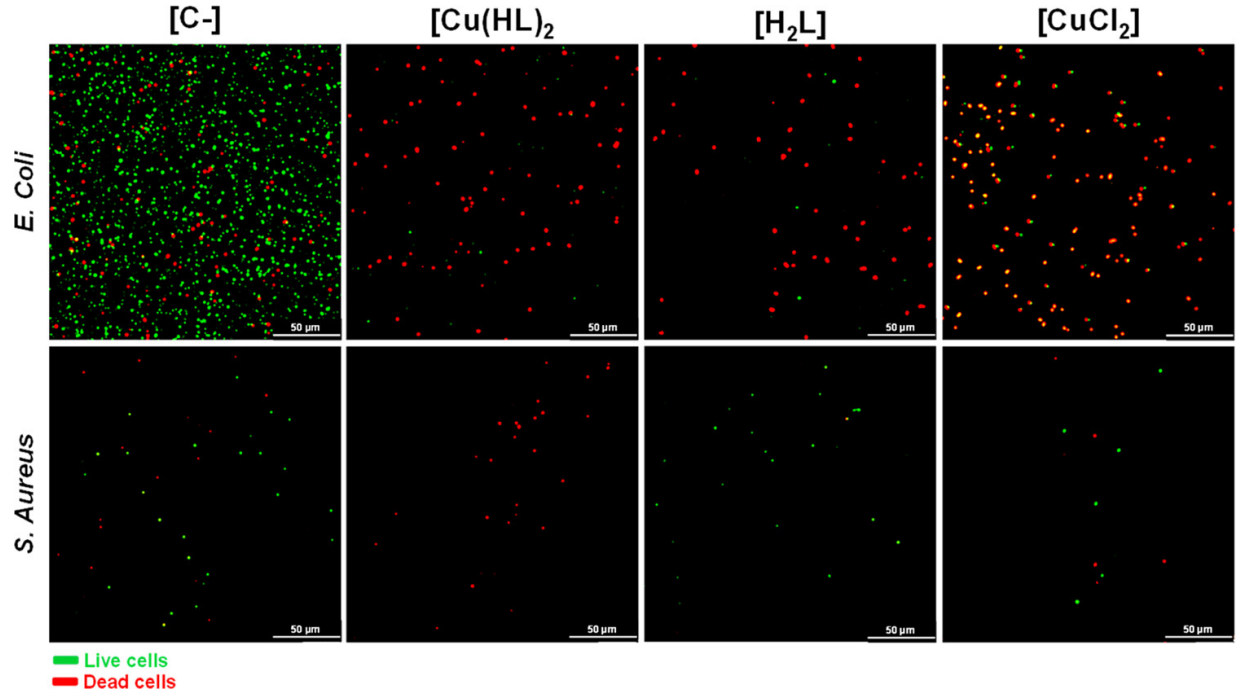

Figure 5: *Fluorescence LIVE/DEAD confocal images of sessile E. coli and S. aureus on cover glass surface after 20 h of contact with the Cu(HL)$_2$ complex at a concentration of 17 µM. Moreover, both strain controls and their complex constituents ($CuCl_2$ and free H_2L ligand) were also depicted for better comparison. The scale bar corresponds to 50 µm. All of the images were taken at 63×.*

This obtained active dose (∼17 μM, providing 22 and 12 % bacterial inhibition) is in the same range of other reported TSCN-copper complexes [10,16]. Thus, the achieved MIC values of the Cu(HL)$_2$ complex seem to be a promising antimicrobial alternative.

Once the antibacterial performance of this metallodrug was evidenced, in an attempt to shed some light on the potential mechanism of action, we performed additional enzymatic (FDA) and oxidative stress evaluation (ROS). ROS production (e.g., HO·, $O_2^{\bullet -}$, HO_2 species) is one of the most recognized growth inhibition processes, resulting in the majority of bacterial death. Hence, a detailed investigation of the antibacterial profile (CFU, FDA) along with the ROS generation of the most responsive dose of this Cu(HL)$_2$ complex was addressed (i.e., 17 μM as the mean value of both strains), compared with the same constituent proportions of the H_2L ligand and the metallic salt ($CuCl_2$). In agreement with previous outcomes, the selected dose was able to inhibit the formation of the SA colonies even at short times (3 h), being statistically significant beyond 20 h (Figure 4).

In the case of the EC bacteria, a minor antibacterial effect was observed, being more remarkable at longer times (6 and 20 h). In addition, it should be noted that here just the copper precursor was able to induce a strong colony decrease in both strains, regardless of the incubation time (100 % inhibition vs 0 % of $CuCl_2$ and H_2L, respectively), pointing out the major role of copper in the antibacterial effect of the complex (Figure 4).

In terms of the potential oxidative stress, the presence of Cu(HL)$_2$ did not seem to be involved in the induced antibacterial effect since no ROS production was observed over time (Figure S6). This specific absence of oxidative species could be related by diverse concomitant factors, such as (i) previously reported data about their ineffectiveness role on the redox activity, (48) (ii) the observed electrochemical behavior (Figure S4) as well as (iii) the influence of the chosen dose (17 μM) or (iv) the duration of the contact time (up to 20 h). On the other hand and regarding the enzymatic activity, the Cu(HL)$_2$ complex led to a relevant inhibition activity in both types of bacteria (±70 and 80 % at SA and EC, respectively), prolonged over time. In the case of the precursors, despite the H_2L ligand did not provide lower CFUs at any time point, it seems to affect the metabolism of both bacteria in a larger extent than the copper salt since a great activity loss was observed, even at shorter times (±90–94 and 93-99 % time fluctuations in SA and EC strains, respectively; Figure S6). Thus, the bactericidal action of the complex could be at least partially explained by its enzymatic repercussion.

For a better understanding of the biocidal effect of Cu(HL)$_2$, the live and dead bacteria were discriminated by LIVE/DEAD staining (green and red labeling, respectively), observed with confocal microscopy at the longest contact time. Remarkably, upon 20 h of

incubation, we evidenced the absence of viability in the few remaining bacteria, decreasing not only the number of live cells but also the dead ones, which suggests a stronger effect coming from the selected dose (Figure 5).

Regarding the precursors' action, both ligand and Cu salt showed a drastic bacterial mitigation (being more significant in *S. aureus*), observing a slight intense yellow color ("milder effect") in the case of copper than the fewer red staining (higher bacterial death rate) in contact with the H_2L linker. Thus, a potential dual effect seems to be evidenced for the achieved complementary action of the intact complex, demonstrating a stronger antibacterial effect against both strains. The higher permeability rate in the case of nonrigid wall of S. aureus could be associated with the time-response effect of each component in contact with each specific bacterial strain, as, for instance, the impact of the lipophilic character. In other words, fluctuations on the component penetration and/or retention rates ("permeability coefficient") could be closely associated with particular molecular descriptors (e.g., molecular mass, hydrophobicity, hydrogen bonding) along with the nature of each bacterial wall structure, displaying here the strongest effect in the case of SA due to the absence of capsule formation in comparison with the rigid cellular wall of *E. coli* [49,50]. Despite the already reported diverse capabilities of bacterial cell lysis and resulting performance efficacies depending on the thiosemicarbazone-derived ligands (e.g., lipopolysaccharide (LPS) instability, membrane disruption), the action mechanism or the associated cellular response remains still unexplored.

6. Conclusions

We have reported the synthesis of a novel effective antibacterial copper–thiosemicarbazone complex, demonstrating their stability, lipophilicity, and performance under simulated physiological media. A significant growth inhibition of $\pm$22 and 12 % in SA and EC after 20 h was, respectively, evidenced, partially related to the enzymatic inhibition observed in both type of bacteria over time ($\pm$70 and 80 % at SA and EC, respectively) and observing, in addition, an absence of viable bacteria by confocal microscopy. Although these preliminary data have been achieved under no cellular infection environment, they clearly indicate the promising application of these TSCN–copper complexes as effective antibacterial agents since an active dose has been evidenced (in the same inhibitory range or lower than other reported complexes or generic antibiotics such as Amoxicillin) m[51], opening new horizons for alternative/unconventional biocompatible therapies of infectious diseases.

Acknowledgements

A.G.Q., A.I.M. and D.F. acknowledge Spanish MINECO under grant PID2019-106220RB100 and PID2022-137373OB-I00. The authors acknowledge the Multifunctional Metallodrugs in Diagnosis and Therapy Network (MICIU, RED2018-102471-T) as well as T.H. thanks the European Union's Horizon 2020 Research and Innovation Programme under the Marie Sklodowska-Curie grant agreement No. 897678.

Nomenclature

AcOH	Acetic acid
ADME	Absorption, distribution, metabolism, and excretion
AMC	Antimicrobial consumption
AMR	Antimicrobial resistance
ATCC	American type culture collection
ATR	Attenuated total reflectance
CECT	Spanish type Microbial culture collection
CFU	Colony-forming units
CH_2Cl_2	Dichloromethane
CLSM	Confocal laser scanning microscopy
$Cu(ClO_4)_2$	Copper(II) perchlorate
DMEM	Dulbecco's modified Eagle medium
DMSO	Dimethyl sulfoxide
EC	*Escherichia coli*
EDTA	Ethylenediaminetetraacetic acid
EtOH	Ethanol
FAB	Fast atom bombardment
FBS	Fetal bovine serum
FDA	Fluorescein diacetate staining
GDP	Gross domestic product
GLASS	Global antimicrobial resistance and use surveillance system
HEWL	Hen egg white lysozyme
H_2L	N1-(4-(dimethylamino)benzylidene)-N4-(4-nitrofenil)thiosemicarbazone
H_2DCF-DA	2′,7′-dichlorodihydrofluorescein diacetate
MALDI	Matrix-assisted laser desorption-ionization
MIC	Minimum inhibitory concentration
MTT	3-(4,5-dimethylthiazolyl-2)-2,5 diphenyltetrazolium bromide
NB	Nutrient broth
NMR	Nuclear magnetic resonance
OD	Optical density
P	Partition coefficient
PBS	Phosphate-buffered solution

PI	Propodium iodide
ROS	Reactive oxygen species
RPMI	Roswell Park Memorial Institute medium
SA	*Staphylococcus aureus*
TSCN	Thiosemicarbazone
TMS	Tetramethylsilane
ZOI	Zone of inhibition

References

1. Global Action Plan on Antimicrobial Resistance. I.; Sixty-Eighth World Health Assembly. Global Action Plan on Antimicrobial Resistance: I; Global Action Plan on Antimicrobial Resistance, 2015.
2. European Centre for Disease Prevention and Control and World Health Organization. Antimicrobial Resistance Surveillance in Europe. 2021 Data; European Centre for Disease Prevention and Control and World Health Organization, 2023.
3. World Health Organization (WHO). Antimicrobial Resistance and the United Nations Sustainable Development Cooperation Framework; World Health Organization, 2021.
4. Djoko, K. Y.; Goytia, M. M.; Donnelly, P. S.; Schembri, M. A.; Shafer, W. M.; McEwan, A. G. Copper(II)-Bis(Thiosemicarbazonato) Complexes as Antibacterial Agents: Insights into Their Mode of Action and Potential as Therapeutics. Antimicrob. Agents Chemother. 2015, 59 (10), 6444-6453, DOI: 10.1128/AAC.01289-15
5. Trondl, R.; Flocke, L. S.; Kowol, C. R.; Heffeter, P.; Jungwirth, U.; Mair, G. E.; Steinborn, R.; Enyedy, E. A.; Jakupec, M. A.; Berger, W.; Keppler, B. K. Triapine and a More Potent Dimethyl Derivative Induce ER Stress in Cancer Cells. Mol. Pharmacol. 2014, 85, 451, DOI: 10.1124/mol.113.090605
6. Pósa, V.; Stefanelli, A.; Nunes, J. H. B.; Hager, S.; Mathuber, M.; May, N. V.; Berger, W.; Keppler, B. K.; Kowol, C. R.; Enyedy, É. A.; Heffeter, P. Thiosemicarbazone Derivatives Developed to Overcome COTI-2 Resistance. Cancers 2022, 14 (18), 4455 DOI: 10.3390/cancers14184455
7. Pavan, F. R.; da Maia, P. I. S.; Leite, S. R. A.; Deflon, V. M.; Batista, A. A.; Sato, D. N.; Franzblau, S. G.; Leite, C. Q. F. Thiosemicarbazones, Semicarbazones, Dithiocarbazates and Hydrazide/Hydrazones: Anti-Mycobacterium tuberculosis Activity and Cytotoxicity. Eur. J. Med. Chem. 2010, 45 (5), 1898-1905, DOI: 10.1016/j.ejmech.2010.01.028
8. Alahari, A.; Trivelli, X.; Guérardel, Y.; Dover, L. G.; Besra, G. S.; Sacchettini, J. C.; Reynolds, R. C.; Coxon, G. D.; Kremer, L. Thiacetazone, an Antitubercular Drug That Inhibits Cyclopropanation of Cell Wall Mycolic Acids in Mycobacteria. PLoS One 2007, 2 (12), e1343, DOI: 10.1371/journal.pone.0001343
9. Souza, R. A. C.; Costa, W. R. P.; Faria, E. D. F.; Bessa, M. A. D. S.; Menezes, R. D.; Martins, C. H. G.; Maia, P. I. S.; Deflon, V. M.; Oliveira, C. G. Copper(II) Complexes Based on Thiosemicarbazone Ligand: Preparation, Crystal Structure, Hirshfeld Surface, Energy Framework, AntiMycobacterium Activity, in Silico and Molecular Docking Studies. J. Inorg. Biochem. 2021, 223, 111543 DOI: 10.1016/j.jinorgbio.2021.111543
10. Dong, X.; Wang, H.; Zhang, H.; Li, M.; Huang, Z.; Wang, Q.; Li, X. Copper-Thiosemicarbazone Complexes Conjugated-Cellulose Fibers: Biodegradable Materials with Antibacterial Capacity. Carbohydr. Polym. 2022, 294, 119839 DOI: 10.1016/j.carbpol.2022.119839
11. Lobana, T. S.; Indoria, S.; Sood, H.; Arora, D. S.; Hundal, G.; Jasinski, J. P. Synthesis and Structures of 3-Nitro-Salicylaldehyde-N-Substituted Thiosem-Icarbazonates of Copper(II): Novel Bio-Active Materials against E. faecalis, E. coli, and K. Pneumoniae. Inorg. Chim. Acta 2021, 521, 120334 DOI: 10.1016/j.ica.2021.120334
12. Lobana, T. S.; Kaushal, M.; Bala, R.; Nim, L.; Paul, K.; Arora, D. S.; Bhatia, A.; Arora, S.; Jasinski, J. P. Di-2-Pyridylketone-N1-Substituted Thiosemicarbazone Derivatives of Copper(II): Biosafe Antimicrobial Potential and High Anticancer Activity against Immortalized L6 Rat Skeletal Muscle Cells. J. Inorg. Biochem. 2020, 212, 111205 DOI: 10.1016/j.jinorgbio.2020.111205
13. Qi, J.; Wang, X.; Liu, T.; Kandawa-Schulz, M.; Wang, Y.; Zheng, X. Synthesis, Antiproliferative Activity and Mechanism of Copper(II)-Thiosemicarbazone Complexes as Potential Anticancer and Antimicrobial Agents. J. Coord. Chem. 2020, 73 (7), 1208-1221, DOI: 10.1080/00958972.2020.1768378
14. Enyedy, É. A.; Petrasheuskaya, T. V.; Kiss, M. A.; Wernitznig, D.; Wenisch, D.; Keppler, B. K.; Spengler, G.; May, N. V.; Frank, É.; Dömötör, O. Complex Formation of an Estrone-Salicylaldehyde Semicarbazone Hybrid with Copper(II) and Gallium(III): Solution Equilibria and Biological Activity. J. Inorg. Biochem. 2021, 220, 111468 DOI: 10.1016/j.jinorgbio.2021.111468
15. Ohui, K.; Afanasenko, E.; Bacher, F.; Ting, R. L. X.; Zafar, A.; Blanco-Cabra, N.; Torrents, E.; Dömötör, O.; May, N. V.; Darvasiova, D.; Enyedy, É. A.; Popović-Bijelić, A.; Reynisson, J.; Rapta, P.; Babak, M. V.; Pastorin, G.; Arion,

V. B. New Water-Soluble Copper(II) Complexes with Morpholine-Thiosemicarbazone Hybrids: Insights into the Anticancer and Antibacterial Mode of Action. J. Med. Chem. 2019, 62 (2), 512-530, DOI: 10.1021/acs.jmedchem.8b01031

16. Jain, P.; Sharma, S.; Kumar, N.; Misra, N. Ni(II) and Cu(II) Complexes of Bidentate Thiosemicarbazone Ligand: Synthesis, Structural, Theoretical, Biological Studies and Molecular Modeling. Appl. Organomet. Chem. 2020, 34 (9), e5736 DOI: 10.1002/aoc.5736
17. Beraldo, H.; Gambino, D. The Wide Pharmacological Versatility of Semicarbazones, Thiosemicarbazones and Their Metal Complexes. Mini-Rev. Med. Chem. 2004, 4 (1), 31-39, DOI: 10.2174/1389557043487484
18. Hidalgo, T.; Fabra, D.; Allende, R.; Matesanz, A. I.; Horcajada, P.; Biver, T.; Quiroga, A. G. Two Novel Pd Thiosemicarbazone Complexes as Efficient and Selective Antitumoral Drugs. Inorg. Chem. Front. 2023, 10, 1986, DOI: 10.1039/D2QI02424A
19. World Health Organization. The Fight against Antimicrobial Resistance is Closely Linked to the Sustainable Development Goals; World Health Organization, 2020.
20. Fang, W.; Lin, L.-R.; Huang, R.-B.; Zheng, L.-S. 1-[4-(Dimethylamino)Benzylidene]-4-(4-Nitrophenyl)Thiosemicarbazide. Acta Crystallogr., Sect. E: Struct. Rep. Online 2007, 63 (1), o112-o113, DOI: 10.1107/S160053680605166X
21. Sheldrick, G. M. SHELXT-Integrated Space-Group and Crystal-Structure Determination. Acta Crystallogr., Sect. A: Found. Adv. 2015, 71 (1), 3-8, DOI: 10.1107/S2053273314026370
22. Clarke, J. M.; Gillings, M. R.; Altavilla, N.; Beattie, A. J. Potential Problems with Fluorescein Diacetate Assays of Cell Viability When Testing Natural Products for Antimicrobial Activity. J. Microbiol. Methods 2001, 46 (3), 261-267, DOI: 10.1016/S0167-7012(01)00285-8
23. Amariei, G.; Kokol, V.; Vivod, V.; Boltes, K.; Letón, P.; Rosal, R. Biocompatible Antimicrobial Electrospun Nanofibers Functionalized with ϵ-Poly-l-Lysine. Int. J. Pharm. 2018, 553 (1), 141-148, DOI: 10.1016/j.ijpharm.2018.10.037
24. Sierra-Serrano, B.; García-García, A.; Hidalgo, T.; Ruiz-Camino, D.; Rodríguez-Diéguez, A.; Amariei, G.; Rosal, R.; Horcajada, P.; Rojas, S. Copper Glufosinate-Based Metal-Organic Framework as a Novel Multifunctional Agrochemical. ACS Appl. Mater. Interfaces 2022, 14 (30), 34955-34962, DOI: 10.1021/acsami.2c07113
25. Nakamoto, K. Infrared and Raman Spectra of Inorganic and Coordination Compounds, 4th ed.; John Wiley & Sons, Ltd, 1986.
26. Kandioller, W.; Theiner, J.; Keppler, B. K.; Kowol, C. R. Elemental Analysis: An Important Purity Control but Prone to Manipulations. Inorg. Chem. Front. 2022, 9 (3), 412-416, DOI: 10.1039/D1QI01379C
27. Ali, M.A.; Dey, K.K.; Nazimuddin, M.; Smith, F.E.; Butcher, R.J.; Jasinski, J.P.; M Jasinski, J.M. The Preparation and Characterization of Some Copper(II) Complexes of the 6-Methyl-2-Formylpyridine Thiosemicarbazone and the x-Ray Crystal Structure of the Chloro(6-Methyl-2-Formylpyridinethiosemicabazonato) Copper(II) Complex. Polyhedron 1996, 15 (19), 3331-3339, DOI: 10.1016/0277-5387(96)00003-4
28. Hosseini-Yazdi, S. A.; Hosseinpour, S.; Khandar, A. A.; Kassel, W. S.; Piro, N. A. Copper(II) and Nickel(II) Complexes with Two New Bis(Thiosemicarbazone) Ligands: Synthesis, Characterization, X-Ray Crystal Structures and Their Electrochemistry Behavior. Inorg. Chim. Acta 2015, 427, 124-130, DOI: 10.1016/j.ica.2014.12.011
29. Allen, F. H.; Watson, D. G.; Brammer, L.; Orpen, A. G.; Taylor, R. Typical Interatomic Distances: Organic Compounds. Int. Tables Crystallogr. 2006, 100, 790-811, DOI: 10.1107/97809553602060000621
30. Fabra, D.; Matesanz, A. I.; Herrero, J. M.; Alvarez, C.; Balsa, L. M.; Leon, I. E.; Quiroga, A. G. Two Different Thiosemicarbazone Tauto-Conformers Coordinate to Palladium (II). Stability and Biological Studies of the Final Complexes. Eur. J. Inorg. Chem. 2021, 2021 (11), 1041-1049, DOI: 10.1002/ejic.202001066
31. Nel, A. E.; Mädler, L.; Velegol, D.; Xia, T.; Hoek, E. M. V.; Somasundaran, P.; Klaessig, F.; Castranova, V.; Thompson, M. Understanding Biophysicochemical Interactions at the Nano-Bio Interface. Nat. Mater. 2009, 8 (7), 543-557, DOI: 10.1038/nmat2442 View Google Scholar 32.

Mitragotri, S.; Burke, P. A.; Langer, R. Overcoming the Challenges in Administering Biopharmaceuticals: Formulation and Delivery Strategies. Nat. Rev. Drug Discovery 2014, 13 (9), 655-672, DOI: 10.1038/nrd4363

33. Fattal, E.; Tsapis, N. Nanomedicine Technology: Current Achievements and New Trends. Clin. Transl. Imaging 2014, 2 (1), 77-87, DOI: 10.1007/s40336-014-0053-3
34. Hall, M. D.; Telma, K. A.; Chang, K. E.; Lee, T. D.; Madigan, J. P.; Lloyd, J. R.; Goldlust, I. S.; Hoeschele, J. D.; Gottesman, M. M. Say No to DMSO: Dimethylsulfoxide Inactivates Cisplatin, Carboplatin, and Other Platinum Com-

plexes. Cancer Res. 2014, 74 (14), 3913-3922, DOI: 10.1158/0008-5472.CAN-14-0247

35. Patra, M.; Joshi, T.; Pierroz, V.; Ingram, K.; Kaiser, M.; Ferrari, S.; Spingler, B.; Keiser, J.; Gasser, G. DMSO-Mediated Ligand Dissociation: Renaissance for Biological Activity of N-Heterocyclic-[Ru(H6-Arene)Cl2] Drug Candidates. Chem. - Eur. J. 2013, 19 (44), 14768-14772, DOI: 10.1002/chem.201303341
36. Prajapati, J. D.; Kleinekathöfer, U.; Winterhalter, M. How to Enter a Bacterium: Bacterial Porins and the Permeation of Antibiotics. Chem. Rev. 2021, 121 (9), 5158-5192, DOI: 10.1021/acs.chemrev.0c01213
37. Fábregas, J.; Vázquez, V.; Cabezas, B.; Otero, A. Tris Not Only Controls the PH in Microalgal Cultures, but Also Feeds Bacteria. J. Appl. Phycol. 1993, 5, 543-545, DOI: 10.1007/BF02182514
38. Lipinski, C. A. Lead- and Drug-like Compounds: The Rule-of-Five Revolution. Drug Discovery Today Technol. 2004, 1 (4), 337-341, DOI: 10.1016/j.ddtec.2004.11.007
39. Glisoni, R. J.; Chiappetta, D. A.; Finkielsztein, L. M.; Moglioni, A. G.; Sosnik, A. Self-Aggregation Behaviour of Novel Thiosemicarbazone Drug Candidates with Potential Antiviral Activity. New J. Chem. 2010, 34 (9), 2047-2058, DOI: 10.1039/c0nj00061b
40. Bellido, E.; Guillevic, M.; Hidalgo, T.; Santander-Ortega, M. J.; Serre, C.; Horcajada, P. Understanding the Colloidal Stability of the Mesoporous MIL-100(Fe) Nanoparticles in Physiological Media. Langmuir 2014, 30 (20), 5911-5920, DOI: 10.1021/la5012555
41. Gabbiani, C.; Massai, L.; Scaletti, F.; Michelucci, E.; Maiore, L.; Cinellu, M. A.; Messori, L. Protein Metalation by Metal-Based Drugs: Reactions of Cytotoxic Gold Compounds with Cytochrome c and Lysozyme. J. Biol. Inorg. Chem. 2012, 17 (8), 1293-1302, DOI: 10.1007/s00775-012-0952-6
42. Casini, A.; Mastrobuoni, G.; Temperini, C.; Gabbiani, C.; Francese, S.; Moneti, G.; Supuran, C. T.; Scozzafava, A.; Messori, L. ESI Mass Spectrometry and X-Ray Diffraction Studies of Adducts between Anticancer Platinum Drugs and Hen Egg White Lysozyme. Chem. Commun. 2007, (2), 156-158, DOI: 10.1039/B611122J
43. Marzo, T.; Navas, F.; Cirri, D.; Merlino, A.; Ferraro, G.; Messori, L.; Quiroga, A. G. Reactions of a Tetranuclear Pt-Thiosemicarbazone Complex with Model Proteins. J. Inorg. Biochem. 2018, 181, 11-17, DOI: 10.1016/j.jinorgbio.2018.01.002
44. Gospodarczyk, W.; Kozak, M. Interaction of Two Imidazolium Gemini Surfactants with Two Model Proteins BSA and HEWL. Colloid Polym. Sci. 2015, 293 (10), 2855-2866, DOI: 10.1007/s00396-015-3671-z
45. Matesanz, A. I.; Jimenez-Faraco, E.; Ruiz, M. C.; Balsa, L. M.; Navarro-Ranninger, C.; León, I. E.; Quiroga, A. G. Mononuclear Pd(II) and Pt(II) Complexes with an α-N-Heterocyclic Thiosemicarbazone: Cytotoxicity, Solution Behaviour and Interaction: Versus Proven Models from Biological Media. Inorg. Chem. Front 2018, 5 (1), 73-83, DOI: 10.1039/C7QI00446J
46. Kowol, C. R.; Heffeter, P.; Miklos, W.; Gille, L.; Trondl, R.; Cappellacci, L.; Berger, W.; Keppler, B. K. Mechanisms Underlying Reductant-Induced Reactive Oxygen Species Formation by Anticancer Copper(II) Compounds. J. Biol. Inorg. Chem. 2012, 17 (3), 409-423, DOI: 10.1007/s00775-011-0864-x
47. Besleaga, I.; Stepanenko, I.; Petrasheuskaya, T. V.; Darvasiova, D.; Breza, M.; Hammerstad, M.; Marć, M. A.; Prado-Roller, A.; Spengler, G.; Popović-Bijelić, A.; Enyedy, E. A.; Rapta, P.; Shutalev, A. D.; Arion, V. B. Triapine Analogues and Their Copper(II) Complexes: Synthesis, Characterization, Solution Speciation, Redox Activity, Cytotoxicity, and MR2 RNR Inhibition. Inorg. Chem. 2021, 60 (15), 11297-11319, DOI: 10.1021/acs.inorgchem.1c01275
48. Noor, A.; Hayne, D. J.; Lim, S.; Van Zuylekom, J. K.; Cullinane, C.; Roselt, P. D.; McLean, C. A.; White, J. M.; Donnelly, P. S. Copper Bis(Thiosemicarbazonato)-Stilbenyl Complexes That Bind to Amyloid-β Plaques. Inorg. Chem. 2020, 59 (16), 11658-11669, DOI: 10.1021/acs.inorgchem.0c01520
49. Kaushik, M.; Sarkar, N.; Singh, A.; Kumar, P. Nanomaterials to Address the Genesis of Antibiotic Resistance in Escherichia coli. Front. Cell. Infect. Microbiol. 2023, 12, 946184 DOI: 10.3389/fcimb.2022.946184
50. Varela, M. F.; Stephen, J.; Lekshmi, M.; Ojha, M.; Wenzel, N.; Sanford, L. M.; Hernandez, A. J.; Parvathi, A.; Kumar, S. H. Bacterial Resistance to Antimicrobial Agents. Antibiotics 2021, 10 (5), 593 DOI: 10.3390/antibiotics10050593
51. Akhavan, B. J.; Khanna, N. R.; Vijhani, P. Amoxicillin. In StatPearls [Internet]; StatPearls Publishing: Treasure Island, (FL), 2024.

Supplementary Information

Proving the antimicrobial therapeutic activity on a new copper-thiosemicarbazone complex

David Fabra[1], Georgiana Amariei[2], Daniel Ruiz-Camino[1], Ángeles Aguilera[1], Ana I. Matesanz[1], Roberto Rosal[2] Adoracion G. Quiroga[1,*], Patricia Horcajada[3,*], and Tania Hidalgo[3,*]

[1]Department of Inorganic Chemistry, Universidad Autonoma de Madrid, Cantoblanco, 28049 Madrid, Spain
[2]Department of Chemical Engineering, University of Alcalá, 28871 Alcalá de Henares, Spain
[3]Advanced Porous Materials Unit (APMU), IMDEA Energy Institute, Ramón de la Sagra 3, 28935 Móstoles-Madrid, Spain

* Corresponding authors: adoracion.gomez@uam.es, patricia.horcajada@imdea.org, tania.hidalgo@imdea.org

Contents

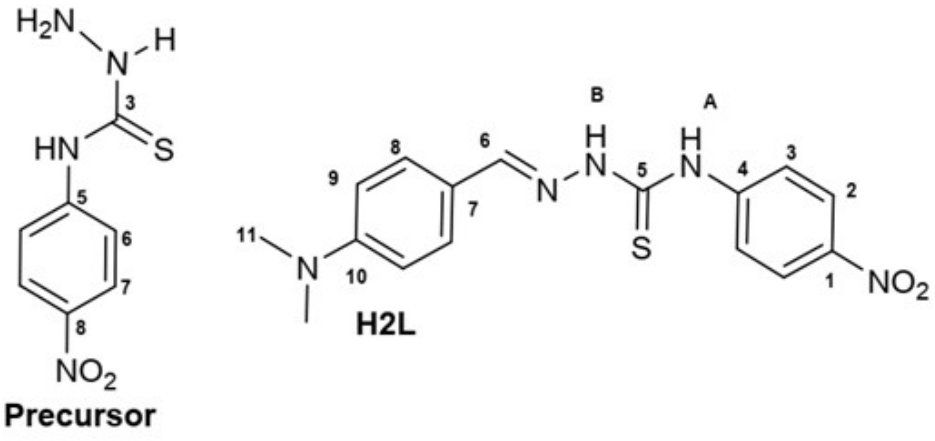

Figure S1: *NMR numbering of the synthesized compounds.*

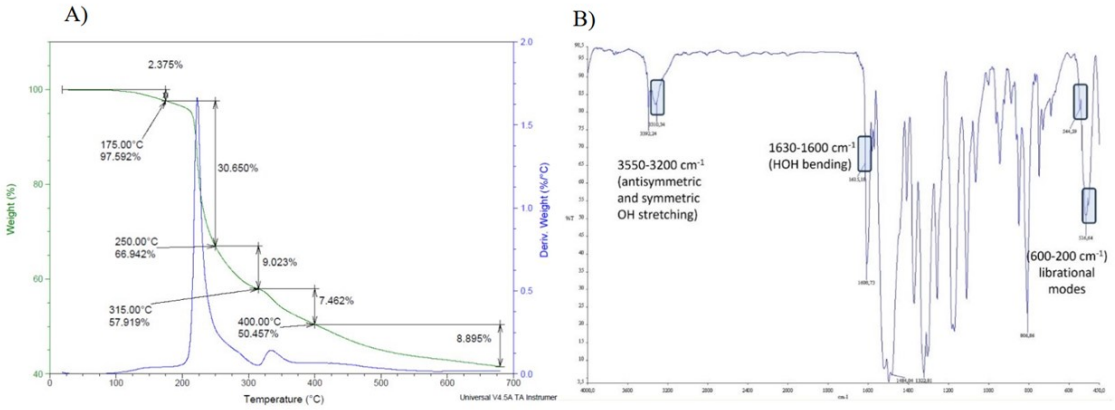

Figure S2: *A) FTIR spectra and B) TGA analysis of $Cu(HL)_2$.*

Table S1. *Particle size (nm) and ζ-potential of $[Cu(HL)_2]$ complex under physiological media.*

	Media	0 h	24 h
Size (nm) [PDI]	H_2O	69 ± 22 [0.2]	76 ± 26 [0.2]
	NB	142 ± 68 [0.6]	241 ± 52 [0.5]
	Cell culture	52 ± 34 [0.5]	125 ± 67 [0.5]
ζ-potential (mV)	H_2O	-22 ± 2	-22 ± 1
	NB	-9 ± 1	-12 ± 1
	Cell culture	-9 ± 1	-10 ± 1

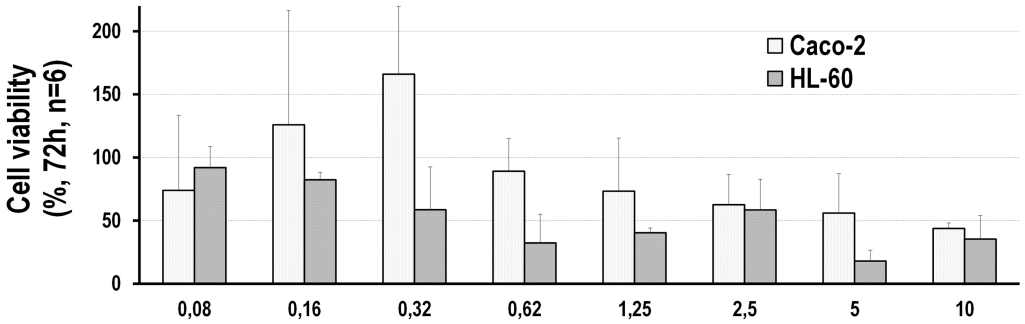

Figure S3: *Cell viability of (A) Caco-2 and (C) HL-60 cell lines after 72 h of incubation with a concentration range of $Cu(HL)_2$ complex. Note that the shown data corresponds to the average of triplicates for each concentration, obtained in two independent experiments (a total of n=6). The vertical error bars drawn in the diagram indicate the range of fluctuations from which the standard deviations were calculated (no statistical significance was detected by the Two-way Anova analysis).*

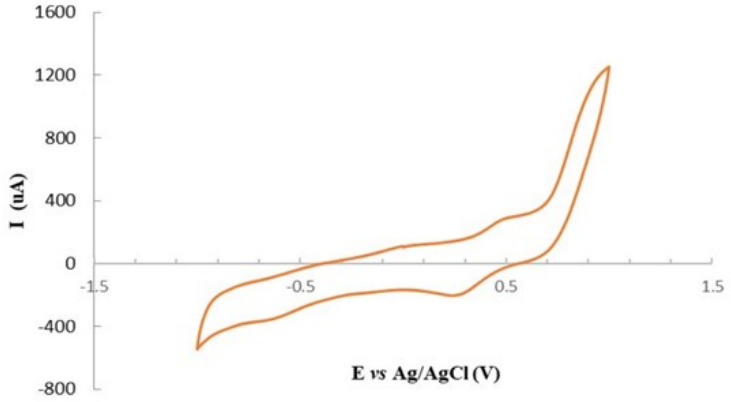

Figure S4: *Cyclic Voltammetry of $Cu(HL)_2$ complex.*

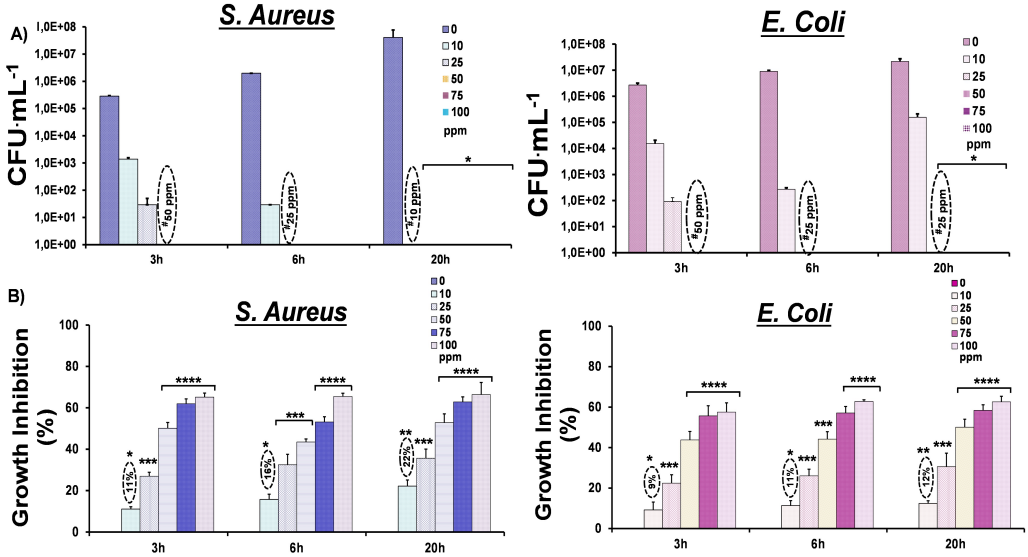

Figure S5: *A) S. aureus (gradient blue columns) and E. coli (gradient red columns) colony-forming units (CFU; indicated as # for minimum inhibitory concentration-MIC) and B) Viability after 3 / 6 / 20 h of contact with a wide range of $[Cu(HL)_2]$ concentrations determined by fluorescein diacetate hydrolysis assay (FDA). In all cases, each sample value was normalized with a negative control (C-, 100 % of bacterial viability). The statistical significance was disclosed as $^*p < 0.05$; $^**p < 0.01$; $^{***}p < 0.005$; $^{****}p < 0.001$..*

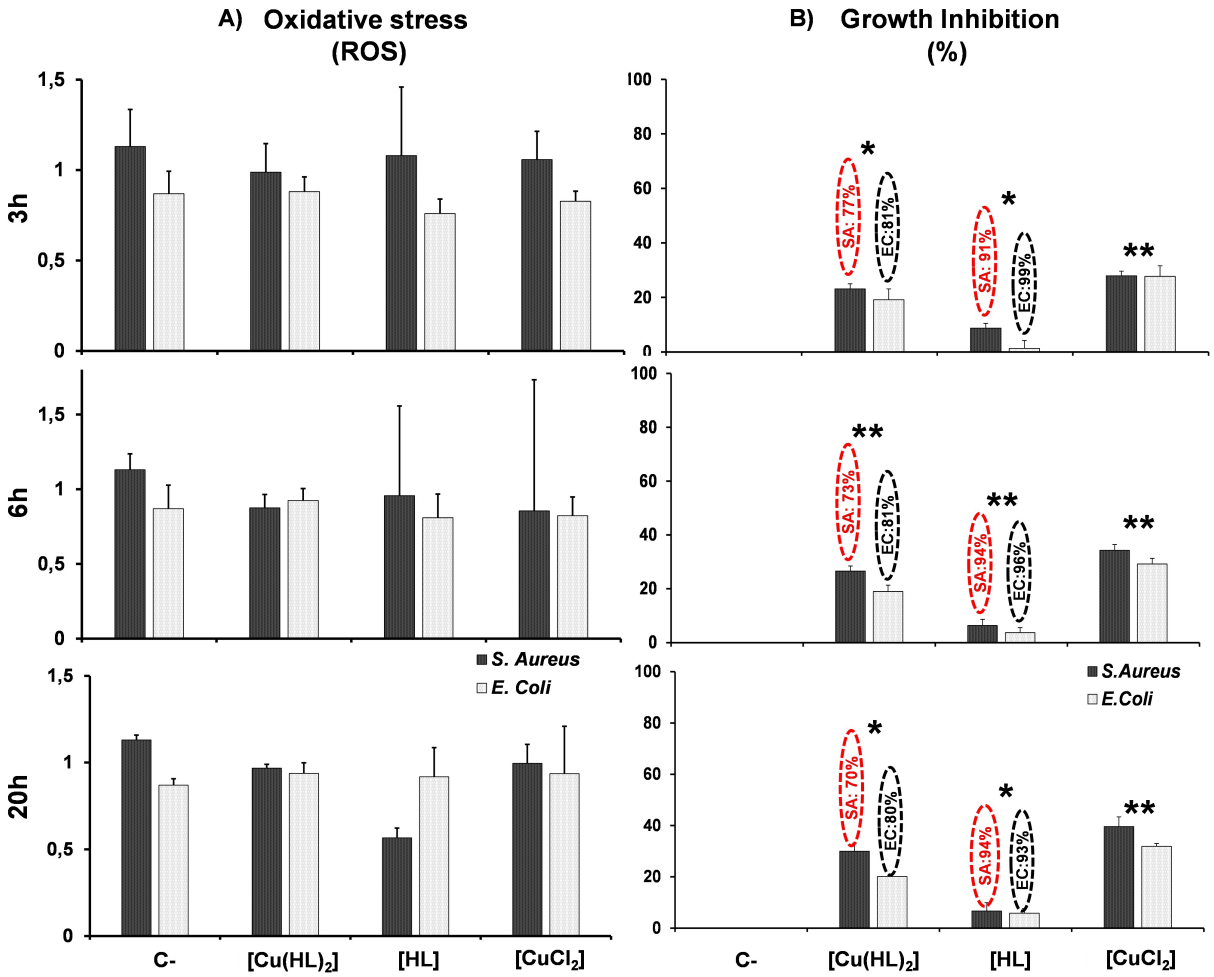

Figure S6: *ROS induction (A) and enzymatic activity loss (%; B) of S. aureus (dark column) and E. coli (white column) after 3 / 6 / 20 h of contact with the selected active [$Cu(HL)_2$; 17 µM] concentration together with the corresponding amount of the following controls: free H2L linker, and $CuCl_2{\cdot}2H_2O$ precursor. In all cases, each sample value was normalized with a negative control (C-, 100 % of bacterial viability). The statistical significance was disclosed as * p <0.05; ** p <0.01.*